Advanced Silicon Avalanche Photodiodes on NASA's Global Ecosystem Dynamics Investigation (GEDI) Mission

Xiaoli Sun*[*a], J. Bryan Blair[a], Jack L. Bufton[b],
Marcela Faina[c], Sigrid Dahl[c], Philippe Bérard[c], Richard J. Seymour[c]

[a]NASA Goddard Space Flight Center, Code 698/61A, Greenbelt, MD, USA 20771;
[b]Global Science & Technology Inc., Greenbelt, MD, USA 20770;
[c]Excelitas Technologies, Vaudreuil-Dorion, QC, Canada J7V8P7

ABSTRACT

Silicon Avalanche Photodiodes (APDs) are used in NASA's Global Ecosystem Dynamics Investigation (GEDI) which was launched in December 2018 and is currently measuring the Earth's vegetation vertical structure from the International Space Station. The APDs were specially made for space lidar with a much lower hole-to-electron ionization coefficient ratio (k-factor ~0.008) than that of commercially available silicon APDs in order to reduce the APD excess noise from the randomness of the avalanche gain. A silicon heater resistor was used under the APD chip to heat the device up to 70°C and improve its quantum efficiency at 1064 nm laser wavelength while maintaining a low dark current such that the overall signal to noise ratio is improved. Special APD protection circuits were used to raise the overload damage threshold to prevent device damage from strong laser return by specular surfaces, such as still water bodies, and space radiation events. The APD and a hybrid transimpedance amplifier circuit were hermetically sealed in a package with a sufficiently low leak rate to ensure multi-year operation lifetime in space. The detector assemblies underwent a series of pre-launch tests per NASA Goddard Environmental Verification Standard for space qualification. They have performed exactly as expected with GEDI in orbit. A detailed description of the GEDI detector design, signal and noise model, and test results are presented in this paper.

Keywords: APD, lidar, space

1. INTRODUCTION

The Global Ecosystem Dynamics Investigation (GEDI) was the latest of a series of space lidar developed at NASA Goddard Space Flight Center (GSFC).[1,2,] GEDI was launched in December 2018 and is currently collecting data from the International Space Station.[3] The GEDI lidar acquires laser pulse waveforms reflected from the vegetation and ground to determine the vertical structure of the tree canopies. Similar to the Laser Vegetation Imaging Sensor (LVIS) on airborne platform,[4] diode-pumped Q-switched Nd:YAG lasers at 1064 nm and 242 Hz[5] with silicon avalanche photodiodes[6] (APD) are used. There are three nearly identical laser transmitters and one of them has its output split into two beams using a Diffractive Optical Element (DOE) forming four beams. Each of the four beams is deflected alternately between two slightly different angles in the cross-track direction. As a result, there is a total of eight ground tracks path at 121 Hz laser pulse rate. The optical signals from the telescope receiver focal plane are coupled to the lidar receivers with multimode optical fibers, each is aligned to a particular laser spot on ground. The lidar receiver consists of six detectors, each can accept signals from two optical fibers or two ground tracks. Four detectors are used for the four ground tracks with the full laser pulse energy and two detectors are used to detect the two pairs of ground tracks with the split laser pulse energy. More details about the GEDI optical design can be found in a separate publication.[7]

The GEDI lidar receivers have to produce high fidelity pulse waveforms over a wide dynamic range in order to provide accurate canopy and vegetation vertical structure. The silicon APDs were specially developed by Excelitas Technologies in Canada for space applications in 1990's and successfully used in a number of space lidar.[1] They have enhanced quantum efficiency at 1064 nm and low excess noise. The original devices used a low-noise high input impedance pre-amplifier and a built-in bias compensation circuit to maintain a near constant responsivity over 0°C to 40°C ambient temperature range. The pre-amplifiers were later upgraded to a wide dynamic range linear transimpedance amplifier (TIA) for the Geoscience Laser Altimeter System (GLAS) on the Ice, Cloud, and land Elevation Satellite (ICESat).[8] A

* xiaoli.sun-1@nasa.gov; phone (301) 614-6732

Thermoelectric Cooler (TEC) was later used to maintain a constant APD temperature and the bias compensation circuit was removed for the BepiColombo Laser Altimeter (BELA).[9] For GEDI, a thin silicon heater is used instead of a TEC to locally heat the Si APD, improving quantum efficiency at 1064 nm laser wavelength without significantly increasing the APD dark noise and the TIA noise. A detailed description of the GEDI detector design, signal and noise model, and measurement results are presented in this paper.

2. SILICON APD FOR THE GEDI LIDAR

GEDI lidar used a set of silicon APDs made by Excelitas Technologies, specially designed for space lidar with low hole-to-electron ionization coefficient ratio or 'k-factor'. The APDs have an active area diameter of 0.8 mm and are optimized for use with a diode-pumped Nd:YAG laser at 1064 nm wavelength. These APDs, named the C30606 series, have k-factor of about 0.008, which is significantly lower than that of Excelitas's commercially available off-the-shelf silicon APDs (C30954 with a k-factor of about 0.02). Specially for GEDI, an integrated silicon heater was used to heat the APD chip to improve quantum efficiency at 1064 nm wavelength.

2.1 APD chip with enhanced response at near infrared wavelength

The APDs have a reach-through structure, which was originally developed by Excelitas Technologies (previously RCA and PerkinElmer), and have the advantage of high quantum efficiency, high gain, and low noise.[10] The absorption layer is relatively thick (~100 microns) compared to other silicon photodiodes. To further improve the quantum efficiency at near infrared wavelength, the top surface of the APDs were patterned to have a series of "dimples" to effectively deflect the incident light and increase its path length through the absorption layer. A reflector is located at the bottom of the APD chip to reflect the unabsorbed light through the absorption layer again. To mitigate the damaging effects of space radiation, the APDs also had an independently biased guard band to prevent the surface dark current originating from the periphery to contribute to the overall noise. Figures 1 and 2 show a photograph of an APD chip and a surface scan at 635 nm of the detector's active area. There is a slight variation in the responsivity due to the dimples. In practice, the light spot on the APD is many times the size of the dimples which results in a near uniform responsivity across the APD active area. The same APD design has been successfully used in all previous NASA space lidar at 1064 nm laser wavelength.[1]
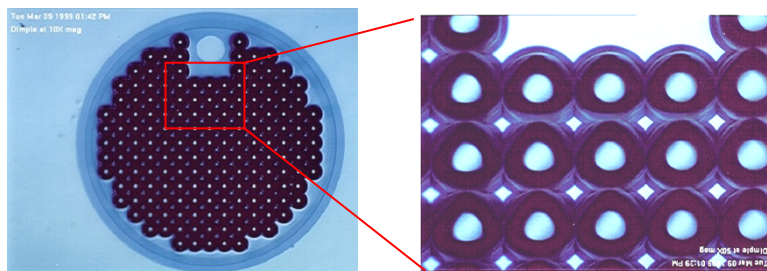

Figure 1. Photograph of an APD chip used in the GEDI lidar
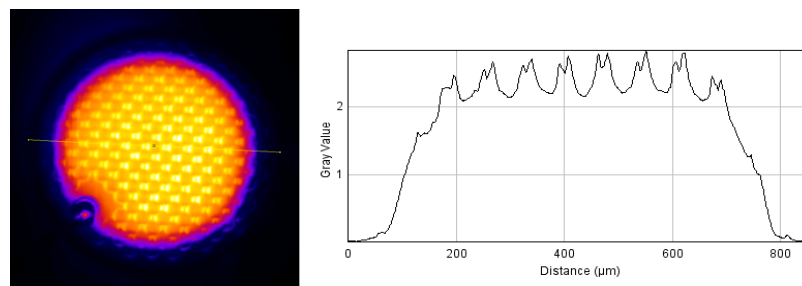

Figure 2. Surface scan of an APD chip used in the GEDI lidar.

The APD has a breakdown voltage of 400 to 450 V at room temperature and a maximum gain of several hundreds. For GEDI, the optimal APD gain was 50 to 100 and the APD bias voltages were set well below the breakdown voltage. We also selected the APDs with a normal operating bias furthest from the breakdown voltage for reliability purposes.

These silicon APDs can withstand multi-year space radiation in lower Earth orbits and even longer in planetary missions.[11,12] They can become deeply saturated when hit by a proton, but recover within a few microseconds with little long-term effects. The lidar measurements can be interrupted briefly if the particle hit coincide with the laser pulses. However, such radiation events are rare in the orbit of the International Space Station.

2.2 Low k-factor to reduce APD gain excess noise

An APD multiplies the primary photocurrent before the subsequent electronic stage. In a well designed system, the electronics noise is relatively small compared to the photo generated noise such that the receiver signal to noise ratio (SNR) is photon noise limited rather than electronic noise limited. However, an APD also introduces excess noise due to the statistical nature of the electron and hole multiplication (gain) within the APD structure. An excess noise factor F is defined as the ratio of the variance of the APD gain and the square of the average APD gain. Ideally the APD gain is deterministic and the excess noise is unity. For silicon APDs, the excess noise factor can be approximated as,[13]

$$F = k_{eff}M + \left(1 - k_{eff}\right)\left(2 - \frac{1}{M}\right) \tag{1}$$

where k_{eff} is a weighted ratio of the hole and electron ionization coefficients and M is the average APD gain. The excess noise reaches a minimum when only electrons are being multiplied in succession inside the APD gain region. In reality, holes travel in the opposite direction and their impact ionizations can result in a larger variation of the secondary photoelectrons generated in the final output. The APD excess noise can be the dominant noise source when the APD is illuminated.

To better understand the beneficial impact of a lower k-factor, the McIntyre APD equation [1] for illuminated noise (i_{ill}) is detailed below,

$$i_{ill} = \sqrt{2q\left(I_{DS} + \left(I_{DB} + I_{pd}\right)M^2\,F\right)} \tag{2}$$

where I_{DS} is the surface dark current, I_{DB} is the bulk dark current, I_{pd} is the primary photocurrent (or the detector unitary responsivity multiplied by the optical power), M is the gain, and q is the electronic charge. By measuring dark current, dark noise, illuminated noise and gain as a function of voltage with a calibrated measurement system at 1064 nm, it is possible to determine the value of the excess noise experimentally at different bias voltages using Eq (2). Figure 3 shows the experimental and theoretical excess noise factor (ENF) as a function of gain for both devices. The APDs specially designed for NASA space lidar, C30606, had a significantly lower ENF than that of the commercial devices, C30954. The two types of APDs are similar in silicon material, device thickness and anti-reflective coating, but the C30606 devices have a different electrical field profile targeting a lower k-factor and consequently a lower ENF.
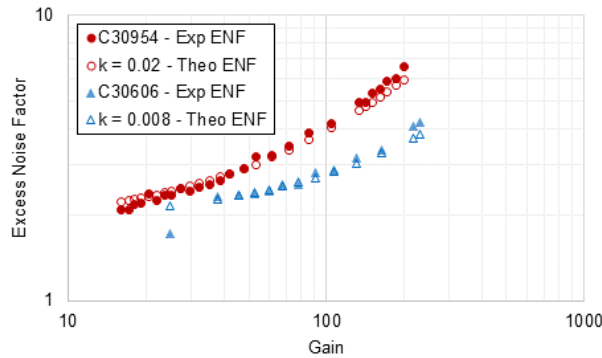

Figure 3. Excess noise factor as a function of gain for the C30606 (low k-factor) and the C30954 (commercial off the shelf) silicon APDs by Excelitas Technologies.

Figure 4 plots the illuminated noise as a function of responsivity using identical test conditions (optical power of 4.5 nW at 1064 nm and room temperature measurements). For comparison purposes, we are also showing what would be obtained for an APD with a k-factor of 0.05, which is typical of high-volume epitaxial Silicon APDs. These APDs normally have a depletion voltage of roughly 50 V compared to 120 V for the C30954 and 250 V for the C30606. We can see that for a given responsivity, or gain of the APD, the lower k-factor results in less noise when the detector is under illumination. This is especially important when the APD is operated with a significant background light level that will be superimposed on the incoming signal.
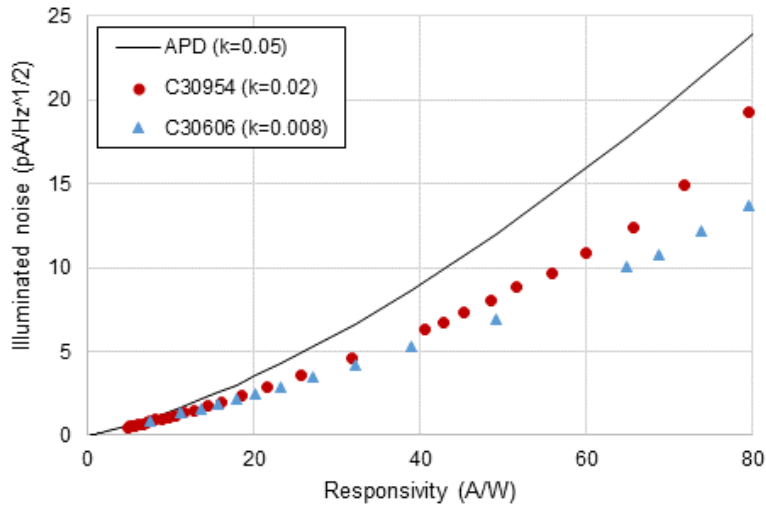
Figure 4. Illuminated noise as a function of responsivity for the C30606, C30954 and a hypothetical 0.05 k-factor APD having similar responsivity at 1064 nm and optical power of 4.5 nW.

2.3 Heating the APD to improve the quantum efficiency at near infrared wavelength

The spectral response of silicon photodiodes beyond 1000 nm depends strongly on the device temperature as shown in Figure 5.[6] Heating the device can significantly improve the quantum efficiency at wavelengths greater than 1000 nm. However, the APD dark current also increases with temperature. It is important for APDs to have a low intrinsic dark current such that raising the device's temperature will be beneficial in terms of SNR. An optimal temperature will then give the best overall performance.
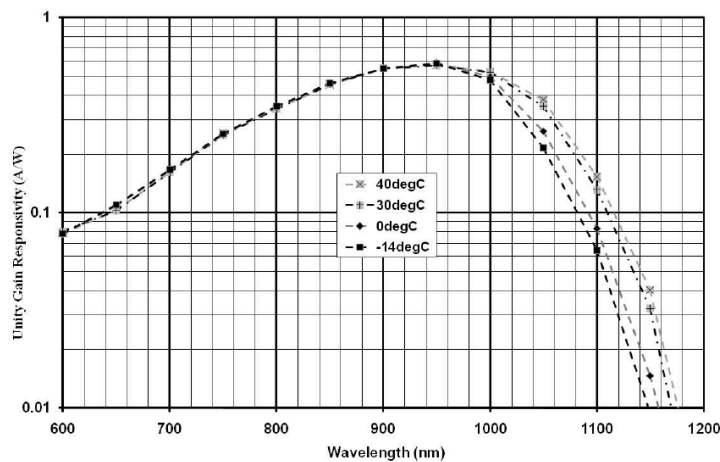
Figure 5. Spectral response of a C30954 series silicon APD. The responsivity decreases rapidlyafter 1000 nm and depends strongly on the temperature.[6]

Figure 6 shows the unity-gain APD responsivity *vs.* temperature and is similar to what was obtained previously.[6] Responsivity can be increased as much as 33% at 1064 nm by heating up the device from room temperature to 70°C
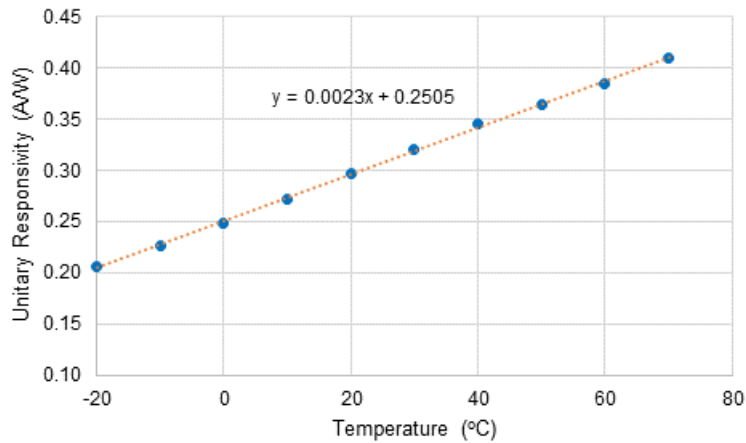

Figure 6. APD unity-gain responsivity as a function of temperature.

The dark current, dark noise, and illuminated noise over this temperature range were also measured and the results are summarized in Table 1 for an operating voltage corresponding to a gain of 100. The APD responsivity increased more rapidly than the noise as the APD temperature increased.

Table I – Measured parameters on the C30606 at a gain of 100 and optical power of 5nW at 1064 nm.

Temperature	Vbd	Vop	Dark current	Dark noise	Illuminated noise	Responsivity
			Gain = 100, P$_o$ = 5 nW			
C°	Volts	Volts	na	pa/√Hz	pa/√Hz	A/W
20	405.8	328.4	0.1	0.1	3.6	29.7
30	429.2	353.6	0.2	0.1	3.8	32.1
40	452.6	377.1	0.5	0.1	4.0	34.5
50	476.1	400.0	1.2	0.2	4.2	36.5
60	499.2	422.5	2.6	0.3	4.3	38.5
70	521.5	445.8	5.5	0.4	4.5	41.0

In practice, it is usually required to maintain a constant APD responsivity, which is the product of the APD quantum efficiency and gain. For a fixed responsivity at 1064 nm, higher device temperature leads to a higher quantum efficiency and lower APD gain, which in turn results in a lower illuminated noise according to Eq. (2). Figure 7 shows the illuminated noise vs. responsivity at different temperature for an optical power of 5 nW. The benefit of heating the APDs is apparent, especially at high responsivity for weak signal detection.
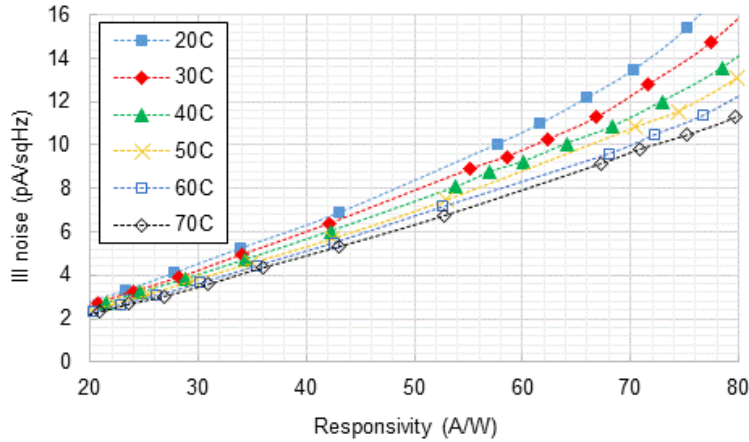
Figure 7. Illuminated Noise as a function of responsivity for the C30606 at different temperature.

Figure 8 shows the calculated overall receiver SNR as a function of the APD temperature for a relatively low optical input (1 nW). The SNR increased with the APD temperature up to 80°C. We chose to set the APD temperature to 70°C for GEDI as a trade-off between the performance, heater power, and thermal design.
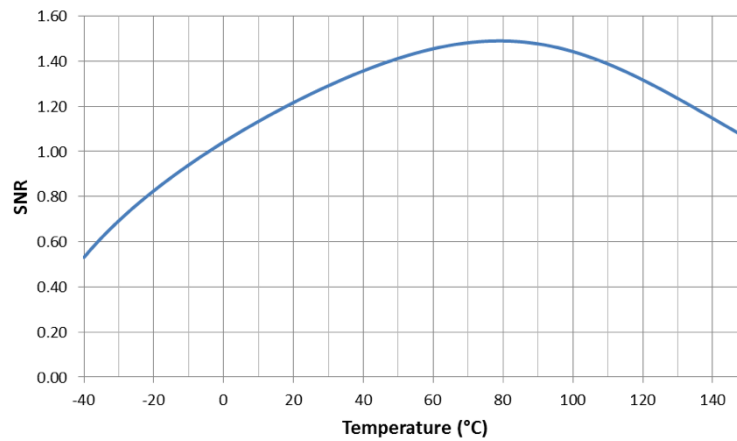

Figure 8. Receiver SNR as a function of the APD temperature.

A silicon heater was used for GEDI instead of a TEC since the APDs only need to heated above its ambient temperature. A silicon chip heater is smaller and can be made to match the size of the APD chip. To minimize the heater power and the preamplifier heating, the APD chips and the heater are thermally isolated through the use of a low thermal conduction spacer. The heater can provide 0.5 W heating power which is sufficient to maintain and regulate the APD temperature to 70°C at an ambient temperature ranging from 15 to 50°C in vacuum. The use of heaters instead of TEC also allows baking the detector modules (unpowered) at higher temperature for cleaning and sterilization required by the planetary protection in future space missions.

2.4 Low noise and high waveform fidelity transimpedance amplifier

A hybrid low-noise transimpedance amplifier (TIA) was integrated with the APD in a hermetically sealed one-inch TO-8 metal package. The TIA had a gain of about 22000 V/A, an equivalent input current noise of < 1.5 pA/Hz$^{1/2}$, and a 3-dB electrical bandwidth of about 100 MHz. The combination of the silicon APD and the transimpedance amplifier gave a responsivity of 540 kV/W and a NEP of < 0.030 fW/Hz$^{1/2}$. Special care was taken to tailor the frequency response of the TIA to give high fidelity pulse waveforms. Figure 9 shows a sample APD module output pulse waveform compared to the laser pulse shape measured by a high-speed PIN photodiode.
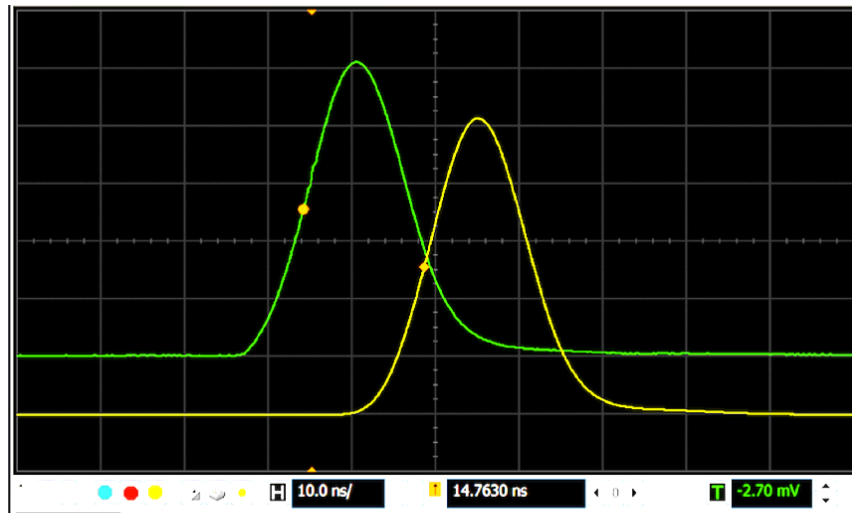
Figure 9. Sample pulse waveforms output from the APD module (yellow) compared
to the laser pulse shape measured by a high-speed photodiode (green).

2.5 Improved damage threshold

A special circuit was included to raise the APD damage threshold to prevent device damage caused by strong laser returns from specular surface and space radiation, especially low energy (~1 MeV) protons which can deposit a large amount of energy and generate up to a million electrons instantly. The voltage drop across the APD decreases when being overloaded, leaving the transimpedance amplifier exposed to the high voltage. Standard commercial silicon APD C30954 has a damage threshold of 1 mW peak optical power. The C30606 APDs for GEDI with the special protection circuit has an estimated damage threshold of greater than 50 mW. The GEDI APD modules were all tested for overload recovery up to 1.0 mW, some of them to 3.0 mW, and they showed no damage or sign of deterioration.

3. DETECTOR ASSEMBLY AND ENVIRONMENTAL TESTING

The silicon APD modules were housed in the detector assemblies which were developed at NASA GSFC. Each detector assembly contained an APD module, an amplifier with a filtering circuit and a power supply. The output signal from each detector assembly is sent over a coax cable to a 12-bit 1 Gs/s waveform digitizer. There were eight flight detector assemblies built and tested. Six units were used in GEDI and two units as the flight spares.

3.1 Detector assembly design and performance measurements

Figure 10 shows a computer aided design (CAD) drawing of the detector assembly. The APD module was rigidly mounted on the detector housing and the optical assembly to maintain optical alignment. The leads of the detector module were connected to the amplifier circuit board with special strain relief to prevent excess force on the leads from thermal expansion which might compromise the hermetic seals of the detector module around the leads. The size of the detector assembly without the optics was 133 x 110 x 58 mm. The mass was 0.85 kg, and the electrical power dissipation was about 4.0 W per detector assembly.
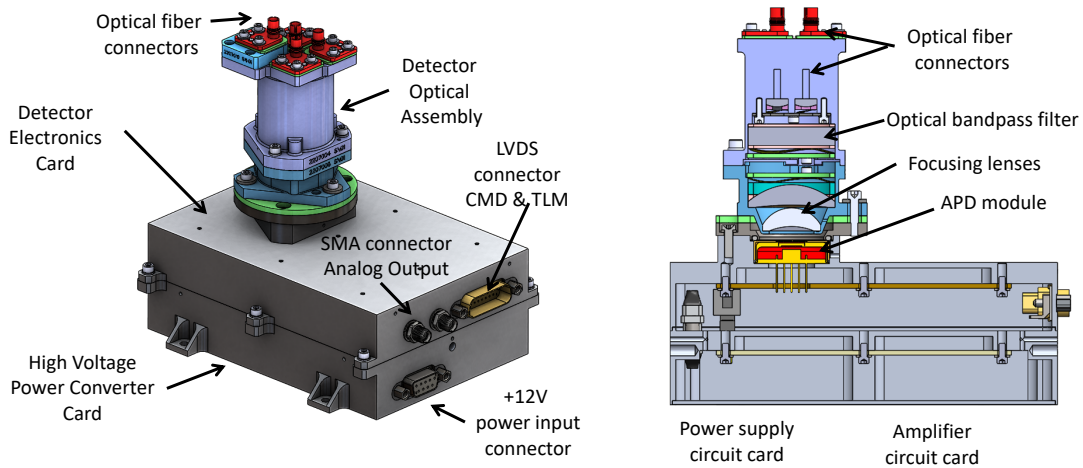
Figure 10. GEDI detector assembly, including the optics, the amplifier circuit, and the power supply circuit.

The detector electronic consists of a buffer amplifier, a lowpass filter, a resistor network for gain adjustment, and a line-driver amplifier for the coax cable to the waveform digitizer. A block diagram of the circuit is shown in Figure 11. The buffer amplifier had a low noise figure such that it was not the dominant noise source. The lowpass filter had a 9-pole Bessel lowpass design with a 3-dB cut-off frequency of 99 MHz. Bessel lowpass filters were chosen to minimize pulse shape distortion. The impulse response of the filter could be approximated as a Gaussian function with roughly 4.5-ns full width at half maximum (FWHM), which was about 1/3 the laser pulse width and should only cause a slight (<10%) pulse broadening for the 12 ns laser pulses. The total voltage gain of the amplifiers was 5.7 considering the factor of 2 loss when driving a 50-ohm coax cable with a 50-ohm output impedance amplifier. The resistor network could be used to reduce the overall amplification gain by a factor of 3 to extend the dynamic range when needed. The signal was AC-coupled with relatively large capacitor to minimize its effect on the output pulse shape.
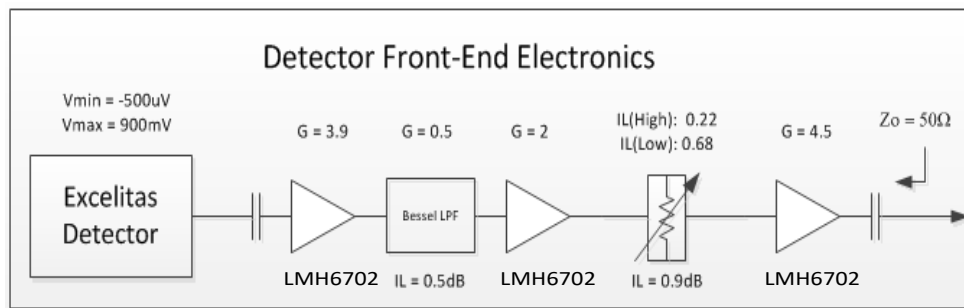

Figure 11. Block diagram of the detector electronics circuit after the APD module

The maximum linear output from the detector assembly was 1.6 V into a 50-ohm load. The combined 3-dB electrical bandwidth was 65 to 70 MHz. The dark noise at the output was about 0.9 mV standard deviation with the amplifier circuit at its full gain. The electronics noise from the buffer amplifier was < 0.4 mV based on the measurement before the APD module integration. The noise floor of the waveform digitizer was less than the noise from the buffer amplifier. Therefore, the dominant noise source was the APD and the transimpedance amplifier, as it should be. This dark noise corresponded to an overall noise equivalent power (NEP) of 0.020 to 0.030 fW/Hz$^{1/2}$. The linear dynamic range of the detector assembly was about 2000 without averaging.

The power supply and the APD temperature control was on a separate circuit card which provided the high voltage APD bias and the low voltages needed by the APD module and the amplifiers. The APD temperature was regulated to 70°C. The APD high voltages were set to give the highest receiver SNR at the set APD temperature. Since the APD breakdown

voltage and consequently the operating bias voltage increased with temperature, the APD could potentially be damaged if the full bias voltage for 70°C operation was applied when the APD is at a much low temperature. To prevent this from happening, the high voltage power supply included an interlock circuit to only apply the full APD bias voltage after it reached 70°C.

3.2 Environmental tests

The GEDI detector assemblies underwent a series of function and environmental testing before integration with the GEDI lidar. These included an electronics circuit function test prior to the APD module integration, a full function and calibration tests after the APD module integration, a temperature test at ambient air pressure, and a temperature cycle test in vacuum (thermal-vacuum test), as required by the Goddard Environmental Verification Standard (GSFC-STD-7000). The detector assemblies also underwent a series of functional and environmental test with the GEDI lidar, which consisted of vibration, electro-magnetic interference and compatibility (EMI/EMC) test, and a thermal vacuum test. The performances of the detector assemblies were monitored with the ground support equipment (GSE) and a comprehensive performance test was repeated throughout the tests to characterize and compare the detector performance under different operating conditions.

The detector assembly vibration test consisted of 3-axes sine-sweep test and a random vibration test. The sine-sweep tests were conducted at 0.1 g from 20 to 2000 Hz to verify there was no residence frequency below 100 Hz. The random vibration tests were conducted to 13 g root-mean-square (rms) up to 2000 Hz in all 3 axes for all the flight detector assemblies and 18 g rms for a qualification unit. A mechanical stress analysis was also conducted using a Finite Element (FE) model, which in combination with the vibration test results verified the detector assemblies could survive the launch with sufficient margin. The vibration test helped to identify a potential fault in the electronics in one of the eight unit, which resulted in some ringing in the output pulse waveform after the test. The rest of the seven units passed the tests without any measurable change in their performances.

The ambient temperature test was conducted at room temperature, -20 and 60°C with a temperature transition rate of about 1°C per minute. A hot power-on at 60°C and a cold power-on at -20°C were conducted. The detector performance and power supply voltages and currents were monitored to verify they were within bonds under these extreme conditions.

The thermal-vacuum tests were conducted after the vibration and the ambient temperature tests to verify the detector reliability and characterize the performance in a space-like operating environment. The temperature ranges for the detector assemblies were 15°C to 40°C operation within the specified performance and -20°C to 60°C operation without damage. The thermal vacuum tests consisted one cycle over the survival temperature range followed by 7 cycles from 10°C to 50°C (5 and 10°C margins below and above the nominal operation temperature range). The detector performance was characterized at 15, 20, 30, 40, and 50°C. The detector assemblies performed nominally throughout the thermal vacuum test.

4. GEDI IN-ORBIT WAVEFORM DATA

GEDI was successfully launched aboard SpaceX-16 rocket on December 4, 2018. The GEDI lidar operated nominally after power on and is currently making science measurement for a two-year planned mission. The lidar receiver performed almost the same as the model prediction based on the detector parameters determined from the pre-launch test data.[14]

Figure 12 shows 100 consecutive return pulse waveforms from one of the six detectors when GEDI flew over the Uyuni salt flat, Bolivia, South America over a clear-sky condition. The area is a dried salt-lake with a near flat ideal diffusive surface. It was used as a primary "ground truth" calibration site for the Ice, Cloud, and land Elevation Satellite (ICESat).[15,16] The GEDI pulse waveforms from this pass over this calibration site were all similar to those measured during pre-launch tests with a slightly longer tail at the pulse trailing edge due to the atmosphere effects. The signal pulse amplitudes were about 1400, which spanned 10 to 11 bits out of 12 bits receiver dynamic range. The noise floor was 1.8 (<1bits), which was the same as that measured during pre-launch testing.
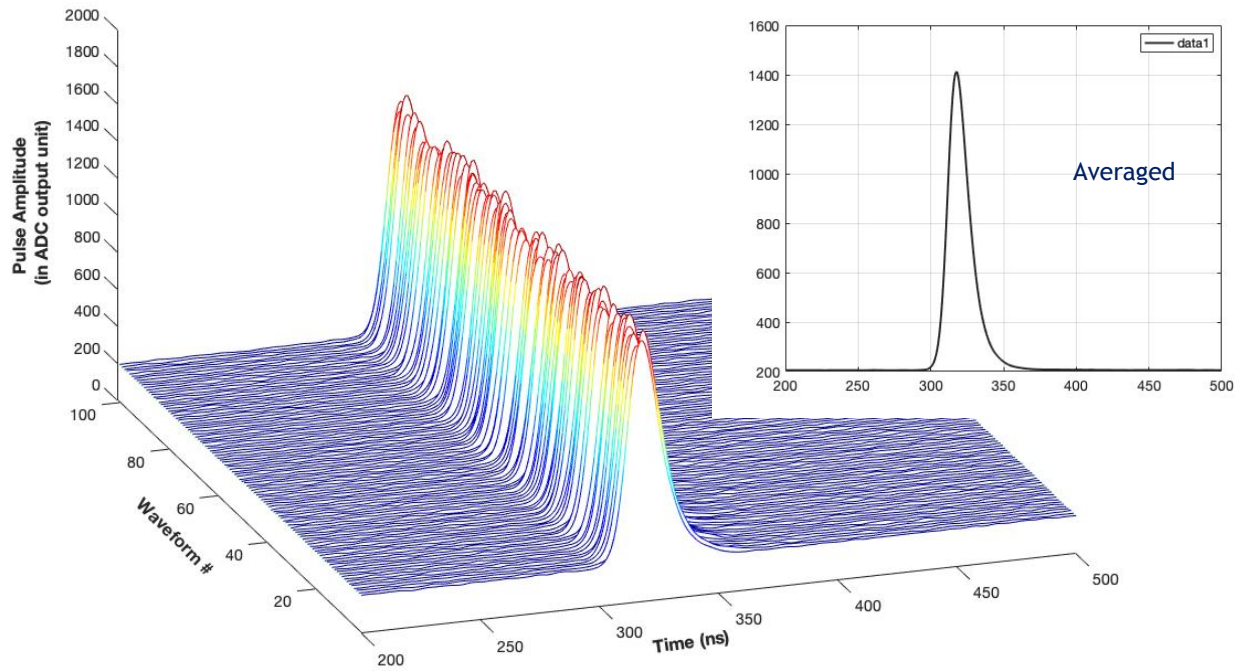
Figure 12. GEDI received pulse waveforms from the Uyuni salt flats, Bolivia, South America, under a clear sky condition. The Uyuni salt flat area was a near ideal diffusive surface with a near 100% reflectance and used for lidar calibration.

Figure 13 shows two GEDI pulse waveforms from a forest area in Gabon, Central Africa, in comparison with the waveforms from the LVIS airborne lidar in a recent campaign at nearly the same laser footprint size and locations. Forests in Gabon are difficult to measure and usually have complex structure due to their dense canopy cover. These GEDI waveforms agreed well with the airborne measurement data. The GEDI calibration and validation program used these and similar data to validate the instrument performance and science data products.
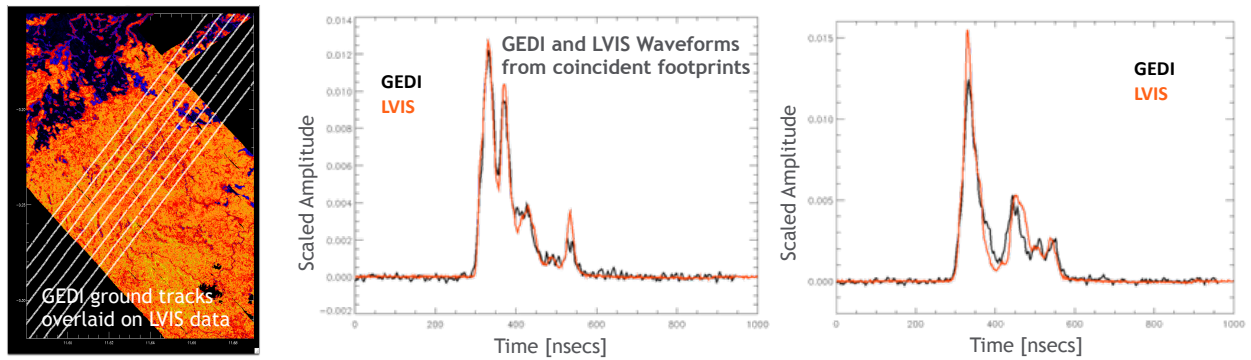

Figure 13. Sample GEDI pulse waveforms from Gabon, Central Africa, in comparison with the waveforms from a recent airborne lidar measurements with coincident footprints.

5. SUMMARY

Advanced silicon APDs were used in the GEDI lidar which was launched in December 2018 to the International Space Station and is currently collecting high quality science data. The APDs were of the reach-through design by Excelitas Technologies and had been used in many previous space lidar in the past. They had a low hole-to-electron ionization coefficient ratio (k-ractor ~0.008) to reduce the excess noise from the avalanche gain process. They also had an enhancen quantum efficiency of about 45% at 1064 nm laser wavelength when heated. A built-in heater was used to heat the APD to $70^{\circ}C$ raising the quantum efficiency while maintaining a low dark current. A hybrid low noise transimpedance amplifier was included inside the detector module. The combination of the silicon APD and the transimpedance amplifier gave a responsivity of 540 kV/W, a NEP of <0.030 fW/Hz$^{1/2}$ and an electrical bandwidth of about 100 MHz. The APD modules were integrated into the detector assembly at NASA GSFC, which included the optics, buffer amplifiers, a matching lowpass filter, and a power supply circuit. The detector assemblies underwent a series of function, performance, and environmental tests per NASA Standard prior integrating to the GEDI lidar. The detector assemblies operated nominally in orbit since launch and performed as expected based on the detector design and prelaunch test results. The return pulse waveform from a near ideal diffusive surface at the Uyuni salt flats were near identical to those from the pre-launch tests. The waveforms from the forest areas in Gabon also agreed with the airborne lidar measurements at the same location and the same footprint size.

ACKNOWLEDGEMENTS

REFERENCES

[1] X. Sun et al., 'Space lidar developed at NASA Goddard Space Flight Center – The first 20 years,' IEEE Selected Topics in Applied Earth Observations and Remote Sensing, 6(3), 1660-1675 (2013).

[2] T. A. Neumann et al., "The ICE, Cloud, and Land Elevation Satellite – 2 mission: A global geolocated photon product derived from the Advanced Topographic Laser Altimeter System," ELSEVIER, Remote Sensing of Environment 223, 11325 (2019)

[3] https://gedi.umd.edu

[4] J. B. Blair, D. L. Rabine, and M. A. Hofton, "The Laser Vegetation Imaging Sensor: A medium-altitude, digitization-only, airborne laser altimeter for mapping vegetation and topography," ISPRS Journal of Photogrammetry & Remote Sensing, 54, 115–122 (1999).

[5] D. B. Coyle et al., "The Global Ecosystem Dynamic Investigation (GEDI) lidar laser transmitter," Proc. SPIE 11128, 111280L (2019).

[6] F. Laforce, "Low noise optical receiver using Si APD," Proc. SPIE 7212, 721210 (2009).

[7] S. Wake et al., "Optical system design and integration of the Global Ecosystem Dynamics Investigation lidar," Proc. SPIE 11128, 111289J (2019).

[8] J. B. Abshire et al., "Geoscience Laser Altimeter System (GLAS) on the ICESat mission: On-orbit measurement performance," Geophysical Research Letters, 32, L21S02 (2005).

[9] N. Thomas et al., "The BepiColombo Laser Altimeter (BELA): Concept and baseline design," ELSEVIER, Planetary and Space Science, 55, 1398-1413 (2007).

[10] A. W. Lightstone, P. P. Webb, and R. J. McIntyre, "Avalanche photodiode," United States Patent 4,654,678 (1987).

[11] X. Sun, P. L. Jester, J. B. Abshire, E. S. Chang, "Receiver Performance Assessment of the Geoscience Laser Altimeter System (GLAS) through the End of Seven-Year Mission in Space," CLEO:2011 (Optical Society of America, Washington, DC, 2011), Presentation ATuA2.

[12] E. B. Clements et al., "Interplanetary Space Weather Effects on Lunar Reconnaissance Orbiter Avalanche Photodiode Performance," AGU Space Weather, 4(5), 343-350 (2016).

[13] R. J. McIntyre, "Multiplication Noise in Uniform Avalanche Diodes," IEEE Transaction on Electron Devices, ED-13(1),164-168 (1966).

[14] S. Hancock et al., "The GEDI simulator: a large-footprint waveform lidar simulator for calibration and validation of spaceborne mission," AGU Earth and Space Science, 6(2), 294-310 (2019).

[15] H. A. Fricker et al., "Assessment of ICESat performance at the salar de Uyuni, Bolivia," Geophys. Res. Lett., 32(21), L21S06 (2005).

[16] X. Sun et al., "ICESat/GLAS altimetry measurements: receiver signal dynamic range and saturation correction," IEEE Trans. Geoscience and Remote Sensing, 55(10), 5440-5454 (2017).